REPORT: BUILDING ENERGY SIMULATION VALIDATION STUDY

IEA ECB ANNEX 71

Ina De Jaeger, Juliana Gonçalves, Christina Protopapadaki, Dirk Saelens

Building Physics Section, Department of Civil Engineering, KU Leuven

26 September 2019

CONTENTS

1 INTRODUCTION

This report describes the modelling methodology and results obtained for the blind phase of the main experiment of the whole model validation exercise carried out in the context of the IEA ECB Annex 71 project. It is accompanied by two result files "Twin_House_Exp1_N2_BWFKULEUVEN_v2.xls" and "Twin_House_Exp1_O5_BWFKULEUVEN_v2.xls". The version number is 2, because some corrections were made after the first submission, following an update in the input data. The exercise was carried out by three modellers, each focusing on different parts of the modelling procedure. However, review of the results, debugging and improvements at a final stage were performed in collaboration with all modellers. The models were developed in Modelica language (v.3.2.2, 2016-04-03 build 3), based on the IDEAS library (v.2.1.0, 2019-02-28) [1]. Simulations were performed in the commercial software Dymola (v. 2018, 2017-04-10) [2], using the "dassl" solver, with 10^{-6} tolerance and output time step of 10 min (the integration step is variable and depends on the dynamics of the system). The 10-minutely data were then averaged to hourly values, so that hour 1 is the average from 00:00 to 01:00.

In the following, Section 2 gives an overview of the implemented models, as well as the assumptions and simplifications made with respect to the specifications. The content of that section is structured following the description in the specification document "Experimental specification BESmodVAL _annex71_v4.6.pdf". In Section 3, the results of the blind phase of the main experiment are presented and evaluated. This phase includes the Co-heating, User 1 and User 2 phases, which took place between 7-12-2018 and 1-3-2019.

2 IMPLEMENTATION AND ASSUMPTIONS

This section provides a description of the models and methods implemented to simulate the twin houses for this experiment. The assumptions, changes and simplifications that have been made with regard to the provided documentation are furthermore highlighted.

2.1 LOCATION AND SURROUNDINGS

The shading caused by buildings surrounding the twin houses is not taken into account, as the model does not consider the 3D geometry of the buildings nor of their surroundings. The impact of surrounding buildings, especially of the additional building to the west of O5, was studied using the shadowing feature of Google SketchUp. The impact is found to be low, as the surroundings only cause shading on the twin houses early in the morning or late in the evening, when the solar irradiation is limited.

Additionally, the documentation states that snow levels can cause shading, particularly on the glass door of the living room. The snow levels are measured at the weather station, which is situated at 50 to 100 m from the twin houses. However, the glass door is situated at the south façade, where increased wind speeds usually reduce the snow level following the documentation. Since no exact data on the snow level at the glass door is available, this shading effect is neglected in the present model, as it is expected to be of minor importance.

2.2 GEOMETRY

The same building structure was modelled for both twin houses. Each room of the ground floor and attic are modelled as separate thermal zones, leading to 10 modelled zones in total. The geometric input data that is used to specify surfaces and volumes was taken from the provided

"Plans_TwinHouses.pdf" file. Outer dimensions were used to calculate the surface areas of the exterior envelope components and the floors, while internal dimensions were used to calculate internal walls and columns, as well as air volumes. The dimensions that are used for the thermal bridge calculations are reported in Section 2.5.

2.3 ZONE MODEL

The Zone component includes an air model that represents the thermodynamic state of the air inside the zone, and models for the distribution of long and shortwave radiation between surfaces. Each of the building components, described in Section 2.4, is connected to the zone model, such that its properties and variables (area, inclination, emissivity and radiative temperature) become available for the zone calculations. The zone model furthermore has fluid ports that connect it with a ventilation system, as well as radiative and convective heat ports, which connect it to a heating system or internal heat gains. Further explanations are given in the following sections, while more detailed descriptions can be found in Refs. [1, 3, 4].

2.3.1 Air model

The air model assumes the air inside the zone is well mixed with a uniform temperature and absolute humidity. Air stratification is thus not included. The state of the air node representing the zone is defined based on the convective heat transfers occurring at the surfaces of building components connected to the zone, as well as the occurring ventilation and infiltration flow rates (see next section for the imposed infiltration). The moist air model employed in the simulations decouples pressure and temperature using a gas law in which pressure and temperature are independent, which often leads to significantly faster and more robust computations. The air is assumed to be not saturated and the specific heat capacities at constant pressure and at constant volume are assumed constant. Furthermore, the influence of humidity is not taken into account.

2.3.2 Air leakage/infiltration

The zone model assumes a perfectly airtight zone, where the air infiltration is known. A fixed mass flow rate, calculated as the air change rate per hour multiplied by the air volume of the zone and the air density (1.2 kg/m^3), is injected into and extracted from the zone. The injected air temperature is equal to the outside temperature. The calculation of the included air change rate per hour for the different zones of the twin houses is described below.

In the documentation, the air change rate per hour (ACH) at a pressure of 50 Pa, or the n_{50}-value, is given for both the ground floor and the entire house and for both underpressure and overpressure. The mean n_{50}-value of under and overpressure is considered in the model. The two houses are modelled separately, each characterised by their own air tightness. Moreover, the air tightness is modelled per floor for each of the two houses. The n_{50}-value for the ground floor is given in the documentation. The n_{50}-value for the attic can be obtained from the n_{50}-values for the entire house and for the ground floor, since the n_{50}-value of a building is calculated as the V_{50}-value divided by the air volume involved in the particular pressurisation test. The airflow rate per hour at a pressure of 50 Pa (V_{50}) for the entire house can be calculated as:

$$V_{50,building} = V_{50,gf} + V_{50,attic}$$

where $V_{50,building}, V_{50,gf}, V_{50,attic}$ are the air flow rate per hour at a pressure of 50 Pa for the entire house, the ground floor and the attic respectively. Including the relation between the n_{50}-value and the V_{50}-value results in:

$$n_{50,building} * V_{building} = n_{50,gf} * V_{gf} + n_{50,attic} * V_{attic}$$

where $n_{50,building}, n_{50,gf}, n_{50,attic}$ are the air change rate per hour at a pressure of 50 Pa for the entire house, the ground floor and the attic respectively, and $V_{building}, V_{gf}, V_{attic}$ are the air volumes for the entire house, the ground floor and the attic respectively. Finally, the n_{50}-value for the attic is calculated as follows:

$$n_{50,attic} = \frac{(n_{50,building} * V_{building} - n_{50,gf} * V_{gf})}{V_{attic}}$$

The results can be found in Table 1 for the two floors of the two houses. All rooms of the same floor are assumed to share the same air tightness. To obtain the air change rate per hour at normal conditions, the n_{50}-value is multiplied by 0.07 for the two floors of the two buildings, following DIN V 18599-2 (E) [5].

Table 1: Calculated n_{50}-values [-/h] and air volumes [m³] that are included in the model, for the two floors of both houses. O5 is the test house. N2 is the reference house.

	n_{50}-value for O5 [-/h]	n_{50}-value for N2 [-/h]	Air volume [m³]
Entire house	1.215	0.870	349.406
Ground floor	1.440	1.190	212.394
Attic floor	0.866	0.374	137.012

2.3.3   Distribution of radiative heat gains

Radiative heat gains in the zone may come from diffuse and direct radiation entering from the windows, or other radiative heat sources, such as radiators or occupants, connected to the radiative heat port of the zone. These gains must then be distributed to the different surfaces connected to the zone, which is done as described below.

The transmitted diffuse solar gains are distributed over the inner surfaces using a weighting method based on the product of area and solar absorptance of the surfaces. The weight factor for each surface is given by:

$$WF = \frac{A_s \alpha_{sw,s}}{\Sigma(A_i \alpha_{sw,i})}$$

where WF is the weight factor, A_s is the area of surface s, and $\alpha_{sw,s}$ is the solar absorptance (shortwave emissivity in IDEAS) of surface s. To distribute the direct solar gains, a fixed fraction is allocated to the floor, equal to its solar absorptance. The remaining part is distributed over all other surfaces, in the same way as the diffuse solar gains.

The internal heat gains due to occupancy are distributed in the same way as the diffuse solar gains, but using the longwave emissivity instead of the solar absorptance.

2.3.4   Longwave radiative heat exchange

The Mean Radiant Temperature Network approach from Carroll [6] is used to compute the radiative heat transfer, in which each surface exchanges heat with a fictive radiant surface, leading to a star resistance network. This model is computationally efficient approach that does not require exact view factors to be known.

2.4 BUILDING COMPONENTS

Each zone model is connected to a number of surfaces, representing the building components that enclose (or lay within) the zone's air body. Depending on the construction materials, the orientation and boundary conditions on the other side of the surface, these building components can be put in four main categories:

- outer walls and roofs, which face the exterior environment on their outer side (outdoor air, solar radiation, long-wage radiation exchange),
- windows, which are like outer walls, but additionally allow solar radiation to be transmitted to the interior of the zone,
- boundary walls, which face prescribed conditions on the outer side, e.g. a given heat flow or temperature, and
- internal walls, which face the interior of the zone on both sides.

Some more details concerning these components can be found in the following sections, where we describe how the different elements of the twin houses were modelled. Note that, for all components, the different material layers are modelled, the properties of which have been taken from the "01_Constructions_TwinHouses.xlsx" file, unless stated otherwise.

2.4.1   Outer walls and roof

The basic outer wall model is connected on the one side with the zone interior (the zone's air), and on the other side to the environmental conditions prescribed by the weather model. Other surfaces share the interior connection to the zone, but may have other conditions on the other side, as described in the following sections. Here some explanation is given about the general heat transfer principles implemented in the outer wall model, which are by extension also valid for all other types of surfaces.

To model thermal conduction through a building component, the layers of different materials are modelled, each consisting of several lumped thermal conductors and heat capacitors connected in series. The model assumes one-dimensional heat conduction, temperature evenly distributed over the surface of the component, and homogeneous and constant material thermal properties. For air cavities in the component, convection and radiation are modelled instead of conduction, using appropriate correlations for vertical or horizontal cavities.

Convective heat transfer on the component's surfaces is taken into using heat transfer correlations, separately for interior and exterior (to the environment) surfaces. In the Interior, convection occurs due to buoyancy effects, while on the exterior forced convection happens due to the wind.

Radiative heat transfer treats shortwave and longwave radiation separately. Longwave radiative exchange occurs inside the zone, as explained in Section 2.3.4, and between the building component and the environment. The latter depends on the outer surface temperature of the component, its longwave emissivity, and an equivalent radiative environmental temperature, based on Walton [7] (p.73). Shortwave radiation causes a heat flow to be injected to the outer wall, which depends on the wall's surface solar absorptance (shortwave emissivity in IDEAS).

For exterior walls, the solar absorptance of the outer layer is assumed to be 0.23, according to the documentation provided for Annex 58. For all internal surfaces finished with plaster or gypsumboard, a value of 0.17 is used accordingly. Longwave emissivity is set to 0.9 for all wall finishing materials.

For the roof component, the U-value calculator on ubakus.de was used as a guide to obtain the desired total thermal resistance of the component (4.63 m²K/W not considering surface resistances [8]). To take into account the presence of rafters between the insulation, the properties of that layer were

altered to match the thermal resistance, weight and heat storage capacity per square meter of the layer calculated by the tool (see Table 2). The roof tiles were included with a longwave emissivity of 0.9 and solar absorptance of 0.63, according to the values given in the Annex 58 specifications of the Twin Houses. The two air layers were modeled as thermal resistances, calculated such that the desired total thermal resistance of the component is achieved.

Table 2: Thermal properties of the roof.

Material	Thickness [m]	Thermal conductivity [W/mK]	Density [kg/m³]	Specific thermal capacity [J/kgK]	Thermal resistance [m²K/W]
Roof tiles	0.010	0.700	2000	1000	0.014
Air layer	0.080	0.480			0.167
Roofing membrane (not modelled)					
Formwork (wood)	0.018	0.130	500	1600	0.138
Mineral wool plus rafters	0.180	0.046	83.33	686.67	3.914
Vapour barrier (not modelled)					
Air layer	0.070	0.480			0.146
Gypsum board	0.0125	0.250	900	1000	0.050
Total					**4.428**

2.4.2 Windows

The windows are modelled as outer walls, with the difference that the absorption by and transmission through the window glazing are taken into account based on the angle-dependent optical properties of the glazing layers. These properties were taken from the specification document for the EN410 spectrum.

The window frame is modelled independently of the glazing, as a single layer wall with given U-value (1 W/m²K). Thermal bridge effects at the glass edge are taken into account as line losses with ψ=0.05 W/mK and edge lengths from the specification document.

The shading on the window glazing from the walls surrounding it (because windows are not placed at the outer surface of the wall) is considered using a "box" type of shading device. The latter combines side fins and an overhang, assumed to be positioned 10cm away from the glazing, and have a depth of 15cm perpendicular to the glazing.

The roller blind casing is not modelled independently, but is modelled as part of the window frame with a U-value of 1 W/m²K. The shading is implemented to block all solar radiation (diffuse and direct). No modification to the U-value of the window is made, and the absorption of solar gains on the screen is not modelled.

2.4.3 Ground floor

The ground floor is modelled as a boundary wall, with a prescribed temperature on the outer side of the component. The provided time-varying temperature of the basement (average of two measurements) was used as input.

For the definition of the material layers of the floor, an average thickness of 24 cm was used for the levelling fill, as assumed in the "01_Constructions_TwinHouses.xlsx" file. The solar absorptance of the screed was assumed to be 0.6, and the longwave emissivity 0.9.

2.4.4   Internal walls, floor and columns

Internal walls between adjacent zones are modelled similar to outer walls, but each face only has interior convection heat transfer with the zone's air, and long-wave radiation exchange with other surfaces of the same zone. Each size is connected to the respective zone. The same model is used for walls as well as the floor between the attic and ground floor.

For the attic floor, the properties of the layers as provided in the "01_Constructions_TwinHouses.xlsx" file were used, except for the specific heat of the EPS boards, for which 20 kg/m^3 were assumed, instead of the given 1300. The dry floor heating system is modelled as a uniform layer with properties from the specifications. As explained in Section 2.7.4, the heat from the pipes is injected between this layer and the FERMACELL dry screen above it. The solar absorptance of the FERMACELL screen was assumed to be 0.6, and the longwave emissivity 0.9.

The columns in the living room, kitchen, bedroom and dining room are modelled as adiabatic walls. These are similar to internal walls, but with no heat transfer to one side. The columns were assumed to be made of concrete and have an exposed internal area of 2m×2.6m (perimeter×height), and thickness of 88cm. The thickness was calculated such that the mass is correct, given the assumed exposed area. Heat transfer away from the zone through the columns is only taken into account as point thermal bridges towards the basement and attic, as described in Section 2.5.

2.4.5   Internal and exterior doors

Doors are generally modelled as wall components, either internal or outer walls. For internal doors that are permanently open, both sides are connected to the same zone to which they open. The occasionally closed doors (kitchen-living, corridor-sleeping and trap door) are connected to both zones, thus assumed to be always closed, given that changing the connections between components and zones is not possible during the simulation. The ventilation slots near the base of the doors are tape-sealed and are thus not modelled. Furthermore, the bottom gap, reported to be about 2 mm on average, is neglected.

The documentation specifies that the internal doors are made from wooden honeycomb board with a thickness of 4 cm with a single pane glazed area of 38.0 x 64.5 cm. The opaque part of the doors is assumed to be 5 mm of light-weight MDF, 30 mm of honeycomb cardboard and 5 mm of light-weight MDF. The assumed thermal properties can be found in Table 3. Since no data on the specific heat capacity of honeycomb cardboard was found, it is assumed to be equal to the specific heat capacity of paper. Due to its limited size, the glazed area is neglected in the model. The door is thus assumed to be fully opaque.

Table 3: Thermal properties of the internal doors.

Material	Thermal conductivity [W/mK]	Specific thermal capacity [J/kgK]	Density [kg/m^3]	Thickness [m]	Source
Light-weight MDF	0.09	1700	500	0.005	[8]
Honeycomb cardboard	0.125	1400	43	0.030	[9]
Light-weight MDF	0.09	1700	500	0.005	[8]

The trap door has a different composition. The documentation specifies that it is composed of 40 mm massive wood, 345 mm air and 20 mm massive wood. The thermal properties of the massive wood are assumed to be equal to those of heavy-weight MDF. All assumed thermal properties can be found in Table 4. Both wooden leaves has a 4-sided rubber seal and are thus assumed to be airtight. As a result, there is no air exchange from the staircase to the air compartment between the wooden leaves nor from the living room to the air compartment.

Table 4: Thermal properties of the trap door (from top to bottom).

Material	Thermal conductivity [W/mK]	Specific thermal capacity [J/kgK]	Density [kg/m³]	Thickness [m]	Source
Heavy-weight MDF	0.13	1700	750	0.040	[8]
Air	0.0241	1008	1.23	0.345	[1]
Heavy-weight MDF	0.13	1700	750	0.020	[8]

The front door is not fully specified in the documentation. Therefore, some assumptions are made. The front door is considered to be composed of one single material, which is 72 mm thick. The thermal conductivity of this material is set to 0.081 W/mK, so the correct U-value of 0.94 W/m²K is obtained. The thermal capacity is assumed to be 1000 J/kgK. The total door is assumed to weigh 50 kg based on typical values [10], therefore, the density is set to 347.2 kg/m³.

2.5 THERMAL BRIDGES

The documentation specifies the linear heat loss coefficients (ψ-values) and the point heat loss coefficients (χ-values) for various thermal bridges that are occurring in the twin houses. These ψ- and χ-values are used to calculate the additional heat flow caused by the thermal bridges. The additional heat flows are calculated per zone and directly injected in the radiative heat ports of the different zones, which are then distributed to the different surfaces as explained in Section 2.3.3. For each zone, the following equation is used:

$$Q_{zone} = \sum_{i=1}^{n} \left(\left(\sum (\psi_k * L_k) + \sum (\chi_l * N_l) \right) * \Delta T \right) \qquad (1)$$

where Q_{zone} is the additional heat flow into the studied zone caused by thermal bridging in W, ψ_k is the linear heat loss coefficient of the linear thermal bridge k in W/(m.K), L_k is the length of the linear thermal bridge k in m, χ_l is the point heat loss coefficient of the point thermal bridge l in W/K, N_l is the number of identical point thermal bridges l, ΔT is the temperature difference between the studied zone and the environment with which the heat is exchanged (other thermal zone, exterior or basement).

An overview of the modelled thermal bridges is presented below. The assumptions and simplifications that are made while modelling these thermal bridges are explained. The order in which the thermal bridges are discussed is identical to the order in which they are included in the documentation. All construction elements are modelled following their external dimensions. Therefore, the calculated ψ- and χ-values according to the external dimensions, as reported in the documentation, are included.

1. Wall-ceiling (TB-01, Figure 12 reported in "3.7 Thermal bridges" of the documentation)
   a. This thermal bridge calculation assumes three different temperatures: the outdoor temperature, the indoor temperature and the attic temperature, that is assumed to be significantly colder than the indoor temperature. Since, in the current experiment, the attic is heated, this thermal bridge between the ground floor and the attic via the

wall-ceiling junction is not included in the current model. The thermal bridge between the indoor environment and the outdoor environment via the wall-ceiling junction is modelled and described later.

2. Wall-wall (TB-02, Figure 13 reported in "3.7 Thermal bridges" of the documentation)
   a. This type of thermal bridge occurs in six rooms of the house. On the ground floor, it is included for the kitchen, the sleeping room, the dining room and the living room. The length of the thermal bridge is measured from the lower edge of the floor between the ground floor and the basement until the middle of the floor between the ground floor and the attic (i.e. 3.21 m). On the attic floor, the thermal bridge is included for the two corners of the child 1 room and the two corners of the child 2 room. The length of the thermal bridge is measured from the middle of the floor between the ground floor and the attic floor until the upper edge of the façade (i.e. 1.02 m). The documentation reports the ψ-values for walls with an insulation thickness of 70 mm and of 120 mm. For two of the corners of each floor, the insulation thickness changes from 120 mm to 70 mm. The ψ-value for such a thermal bridge is not reported in the documentation. Hence, the mean of the ψ-value for 120 mm and the ψ-value for 70 mm is included.

3. Wall-floor (TB-03, Figure 14 reported in "3.7 Thermal bridges" of the documentation)
   a. This thermal bridge calculation assumes three different temperatures: the outdoor temperature, the indoor temperature and the basement temperature, that is assumed to be significantly colder than the indoor temperature. In the current experiment, the basement is cold. Therefore, this thermal bridge is included. It is chosen to split the ψ-value in two, i.e. the ψ-value from the ground floor to the outdoor environment and the ψ-value from the ground floor to the attic. The thermal bridge only influences the kitchen, the doorway, the sleeping room, the bath room, the dining room and the living room on the ground floor. These rooms lose heat to both the outdoor environment and the basement during the heating season. The reported ψ-value is multiplied by -1 as the heat flows in this work are defined as towards the room. The lengths of the thermal bridges are calculated based on external dimensions and are reported in Table 5.

4. Ridge (TM-01)
   a. This type of thermal bridge only occurs in the children's rooms. The lengths of the thermal bridges are calculated based on external dimensions and are reported in Table 5.

5. Rake – mineral wool (TM-02-2)
   a. This type of thermal bridge only occurs in the child 1 room. The length of the thermal bridges is calculated based on external dimensions and is reported in Table 5.

6. Rake – PUR (TM-03-2)
   a. This type of thermal bridge only occurs in the child 2 room. The length of the thermal bridges is calculated based on external dimensions and is reported in Table 5.

7. Eaves – combined (TM-04)
   a. It is chosen not to use this thermal bridge calculation, but to split the thermal bridge into two parts (TM-05 and TM-06).

8. Eaves – isolated (TM-05)
   a. This type of thermal bridge occurs in the north and the south façade of the children's rooms and the staircase. The length of the thermal bridges is calculated based on external dimensions and is reported in Table 5.

9. Ceiling - wall (TM-06)

    a. This type of thermal bridge occurs in the north and the south façade of the children's rooms and the staircase. To isolate the heat flow into the rooms of the attic floor, the ψ-value is divided into two. The length of the thermal bridges is calculated based on external dimensions and is reported in Table 5.

10. Column - floor (TM-07)

    a. This point thermal bridge occurs in four rooms of the house (i.e. kitchen, sleeping room, dining room and living room). The specific positions of the columns are obtained from the documentation of the first common exercise.

11. Column - ceiling (TM-08)

    a. This point thermal bridge occurs in four rooms of the house (i.e. kitchen, sleeping room, dining room and living room). The specific positions of the columns are obtained from the documentation of the first common exercise. The columns of the kitchen and the living room are under the child 1 room, whereas the columns of the sleeping room and the dining room are under the child 2 room.

12. Internal wall, thin - Ceiling (TM-10)

    a. Although this thermal bridge will not have a large influence due to the similar temperature in the ground floor and the attic, it is included in the model. The ψ-value is divided into two to differentiate the heat flow from for example the child 2 room to the hall and to the sleeping room. The opposite heat flow to the child 2 room is included as well. The length of the thermal bridges is calculated from the inside of the external wall until half of the junction with other internal walls. An overview of the lengths is reported in Table 5.

13. Internal wall, thin - Floor (TM-11)

    a. Again, the ψ-value is divided into two to differentiate the heat flow for example from the hall and the sleeping room to the basement. The length of the thermal bridges is calculated from the inside of the external wall until half of the junction with other internal walls. As there is a 2mm gap between the internal doors and the floor, their length is not included. An overview is reported in Table 5.

14. Internal wall, thick - Ceiling (TM-12)

    a. Although this thermal bridge will not have a large influence due to the similar temperature in the ground floor and the attic, it is included in the model. The ψ-value is divided into two to differentiate the heat flow from for example the child 1 room to the kitchen and to the living room. The opposite heat flow to the child 1 room is included as well. The thick internal wall that runs from north to south is not included in the thermal bridges, since there is a wall located on top of this wall in the attic floor and thus its impact will be limited. The length of the thermal bridges is calculated from the inside of the external wall until half of the junction with other internal walls. An overview of the lengths is reported in Table 5.

15. Internal wall, thick - Floor (TM-13)

    a. Again, the ψ-value is divided into two to differentiate the heat flow for example from the kitchen and the living room to the basement. The length of the thermal bridges is calculated from the inside of the external wall until half of the junction with other internal walls. As there is a 2mm gap between the internal doors and the floor, their length is not included. An overview is reported in Table 5.

16. Window jamb - brick wall with wood fibre insulation (TM-14)

    a. This type of thermal bridges occurs in the north and south façade of the doorway, the sleeping room, the dining room and the living room. It is also included for the jambs of the doors. An overview of the lengths is reported in Table 5.

17. Window lintel - brick wall with wood fibre insulation (TM-15)
    a. This type of thermal bridges occurs in the north and south façade of the doorway, the sleeping room, the dining room and the living room. It is also included for the jambs of the doors. An overview of the lengths is reported in Table 5.
18. Window sill - brick wall with wood fibre insulation (TM-16)
    a. This type of thermal bridges occurs in the north and south façade of the doorway, the sleeping room, the dining room and the living room. It is also included for the jambs of the doors. An overview of the lengths is reported in Table 5.
19. Window jamb - brick wall with mineral wool insulation (TM-17)
    a. This type of thermal bridges occurs in the west façade of the kitchen, the living room and the child 1 room. An overview of the lengths is reported in Table 5.
20. Window lintel - brick wall with mineral wool insulation (TM-18)
    a. This type of thermal bridges occurs in the west façade of the kitchen, the living room and the child 1 room. An overview of the lengths is reported in Table 5.
21. Window sill - brick wall with mineral wool insulation (TM-19)
    a. This type of thermal bridges occurs in the west façade of the kitchen, the living room and the child 1 room. An overview of the lengths is reported in Table 5.
22. Window jamb - brick wall with PUR insulation (TM-20)
    a. This type of thermal bridges occurs in the east façade of the bath room and the child 2 room. An overview of the lengths is reported in Table 5.
23. Window lintel - brick wall with PUR insulation (TM-21)
    a. This type of thermal bridges occurs in the east façade of the bath room and the child 2 room. An overview of the lengths is reported in Table 5.
24. Window sill - brick wall with PUR insulation (TM-22)
    a. This type of thermal bridges occurs in the east façade of the bath room and the child 2 room. An overview of the lengths is reported in Table 5.
25. Trap door – ceiling (TM-23)
    a. This type of thermal bridges occurs between the living room and the stair case. The length is equal to the perimeter of the trap door and is reported in Table 5.
26. TU-01 – TU-07
    a. These thermal bridge calculations show the u-values from all components. As these U-values are very close to the calculated u-values, it is chosen not to include them in the model.

Table 5: Overview of the included thermal bridges.

Base room	Adjacent space	Total impact due to thermal bridging [W/K]
Kitchen		
	External	-0.52
	Basement	1.02
	Staircase	-0.27
	Child 1	-2.33
Child 2		
	External	1.40
	Sleeping	-3.91
	Hall	0.17
	Bathroom	-1.58

	Dining	-3.91
Doorway		
	External	0.08
	Basement	0.92
	Staircase	-1.12
Sleeping		
	External	-0.57
	Child 2	-3.27
	Basement	1.23
Hall		
	Child 2	0.17
	Basement	0.95
Bathroom		
	External	-0.04
	Child 2	-1.58
	Basement	0.66
Dining		
	External	-0.57
	Child 2	-3.27
	Basement	1.28
Living		
	External	-0.37
	Basement	1.60
	Staircase	0.28
	Child 1	-5.89
Staircase		
	External	0.25
	Kitchen	-0.27
	Doorway	-1.12
	Living	0.28
Child 1		
	External	1.24
	Kitchen	-2.97
	Living	-6.53

Although this list is very detailed, it does not yet take into account all thermal bridges that are occurring in the house: the linear thermal bridge between the skylight and the roof, the linear thermal bridge around the internal doors, the linear thermal bridges around the wall on the attic floor (connection to the roof and to the floor), the linear thermal bridge from the thick internal wall on the ground floor and the thinner internal wall on the attic floor. Although some of these are similar to the provided data, it is chosen not to model them.

2.6 VENTILATION

In the experiment, air circulation between the different rooms occurs, which is defined by the ventilation system on the one hand, and by the opening of doors and windows on the other hand. The

effect of opening the window in room child 1 is treated in Section 2.8.4. However, since the intra-room air exchange was not available from the tracer gas experiment, the implemented model assumed no air movement from/to zones that were not equipped with a supply or extraction fan of the ventilation system. For more details on the treatment of internal doors, see Section 2.8.5.

The implemented model uses an ideal flow source with prescribed values of flow rate and temperature that is connected to the zone fluid ports of rooms where the ventilation supply points are located (living room, child 1 and child 2 rooms). The given supply air temperature and the averaged value of the supply and exhaust flow rates are used as time dependent inputs. For the ground floor, it is assumed that the airflow from the living room continues on to the corridor, and then splits in half to the bathroom and dining room. Since the zone air model assumes a perfectly mixed air volume, the air flowing from one room to the other has the temperature of the former room. At the exhaust points, the air simply exits the circuit into a fixed boundary sink. As already mentioned, no air circulation is modelled to/from the kitchen, doorway, sleeping room or staircase.

The power consumption of the fans and heaters is not used in the model, since their heating effect is already taken into account in the supply air temperatures, which are measured after the fan and heater.

2.7 HEATING

2.7.1 Electric heating

Electric heaters are used in both buildings during the Co-heating phase, and in house N2 for the rest of the experiment, phases User 1 and User 2. Exceptionally, in house O5 electric heating was also active for a short period of malfunctioning, see further. The electric heaters are controlled to keep the set temperatures with a PI controller, based on the measured air temperatures in each room.

In the model, a limited PI controller is implemented using Modelica.Blocks.Continuous.LimPID from the Modelica standard library, with gain equal to 4 and integration time of 5 min, as in the specification, and a limited output between 0-2000W. The zone air temperature (same temperature for the entire volume), and the time-varying prescribed set points are used as inputs to the controller. Note that the malfunctioning in house O5 on December 24th and 25th was also implemented as electric heating with a set point of 21°C from 24.12.2018 07:00 until 25.12.2018 11:00. The required heat input is then split into a radiative and convective part (fixed split 30-70%), and injected into the respective radiative and convective heat ports of the zones as "prescribed heat flows". As such, the dynamics of the heater have been ignored. This assumption can be justified by the fast response time of the heater (estimated as 1 or 2 minutes according to the documentation) with regard to the 10-minutely output.

During the User 1 and User 2 phases, the heaters are also used to provide the artificial internal heat gains. In this case, the prescribed heat flow is the one provided as input, again split as 30% radiative and 70% convective heat. More details on the internal heat gains are given in Section 2.8.1.

2.7.2 Heat pump

The heat pump is not explicitly included in the model. Instead, the measured supply temperatures and flow rates are used as input to the underfloor heating model, see Section 2.7.4.

2.7.3 Domestic hot water

The domestic hot water information was not relevant to the model, since it was chosen not to explicitly model the heat pump.

2.7.4   Underfloor heating

The underfloor heating system is active in house O5 during User 1 and User 2 phases. The model by Koschenz and Lehmann [11] is used to simulate the dynamic behavior of the embedded pipe circuits for both the ground floor and the attic floor. This model corresponds to a concrete core activation floor heating and treats the pipe circuits as heat exchangers. Convective and conductive resistances are estimated based on material properties, the diameter and the spacing of the pipes, and the position of the pipe in the concrete slab. Since the heat pump is not modelled in detail, the measured supply temperatures and flow rates are used as boundary conditions to the underfloor heating model. The return temperature is obtained from the balance between the heat demand of each room, the heat transfer resistance imposed by the floor heating system, and the (measured) supply conditions (which also differ among rooms).

In order to use this model, some characteristics of the floor heating have been simplified. First, no distinction is made between spiral pipes and serpentine pipes. Second, for the rooms with more than one circuit (living, child 1 and child 2), the total mass flow rate is split over the multiple circuits. Third, The size difference among the (sub-)circuits in child 1 and child 2 rooms has been neglected and, therefore, (sub-)circuits are considered to be the same size. Four, the heat transferred from the embedded pipe model to the floor element is injected between two layers. Due to restrictions in the model, the vertical location of the pipes has been adapted for the ground floor system. The pipes are considered to be placed within the screed layer at 0.03 m from the surface. To simulate this situation, two screed layers have been created, one with 0.03 and the other with 0.035 m, and the heat flux is injected between them. For the attic floor, the heat is injected between the FERMACELL dry screen and the floor heating layer, which was modelled as a uniform layer with the properties given in "01_Constructions_TwinHouses.xlsx".

2.8   Synthetic user

2.8.1   Internal heat sources

The internal heat gains are a result of the synthetic artificial occupants and are provided as measured heat loads. Since these gains are implemented by means of the electrical heaters, the same approach is used as in Section 2.7.1 to model the heat that is injected in the zones, only this time using the provided time series as heat load.

Since a malfunctioning occurred in the beginning of User 1 phase, the internal heat loads for house O5 are the sum of the values given in columns "o5_aroom_XX_IHS_elP" and "o5_aroom_XX_heat_elP". For house N2, the values from column "n2_aroom_XX_heat_elP" were only added to the corridor, doorway and staircase, because for these rooms the provided data lasted for less than 3 days, about the duration of the malfunctioning. This contradicts the statements that "the doorway and stairs have no heat input after the co-heating phase", but it could be attributed to the malfunctioning. For other rooms in N2, only column "n2_aroom_XX_IHS_elP" was used.

For the malfunctioning in house O5 on December 24th and 25th, no additional internal gains were applied, but electric heating was implemented instead, as described in Section 2.7.1.

A constant heat gain was furthermore added to the corridor and children's rooms of house O5, which represent gains from the underfloor heating flow meters. According to the specification, 28.8W were added to the corridor, and 2.4W in each of the children's rooms.

2.8.2 Internal humidity sources

Internal humidity sources are not included in the current phases of the experiment.

2.8.3 Set temperatures

Set point temperatures for the electric heaters are read for each room as time-varying inputs from the provided data. When the heaters are off, the set point is lowered to 0 °C. For the floor heating, the set points were not used, since the provided flow rates and supply temperatures were used instead.

2.8.4 External window opening

2.8.4.1 Modelling

During the experiment, a window is opened in the Child1 room, causing an additional ventilation airflow. The ventilation airflow rate through the window, as modelled, takes into account both wind and stack effects.

The volumetric airflow rate resulting from wind effects Q_w is calculated as:

$$Q_w = C_p A_{op} U$$

where C_p is the opening effectiveness, A_{op} is the opening area, and U is local wind speed.

The opening effectiveness, C_p, is given as a function of the angle between the wind flow and the normal to the building façade, ϕ [12]:

$$C_p(\phi) = 0.55 - \left(\frac{\phi}{180}\right) 0.25$$

where ϕ is an angle between 0 and 180 degrees. If the difference ϕ is greater than 180, the difference is set to -180 degrees. This equation is a linear interpolation that gives 0.5 to 0.6 for perpendicular winds and 0.25 to 0.35 for diagonal winds. The same model is used in EnergyPlus.

The local wind speed, U, is calculated from the meteorological reference wind speed, U_{met}, as follows [13]:

$$U = U_{met} \left(\frac{\delta_{met}}{z_{met}}\right)^{a_{met}} \left(\frac{z}{\delta}\right)^{a}$$

where z_{met} is the height of the meteorological wind speed measurement, z is the height of the centroid of the system, and a and δ are terrain-dependent coefficients (Table 6).

Table 6: Terrain-dependent parameters [13].

Terrain	Description	Exponent a [-]	Layer thickness δ [m]
1	Flat, open country	0.14	270
2	Rough, wooded country	0.22	370
3	Towns and cities	0.33	460
4	Ocean	0.10	270
5	Urban, industrial, forest	0.22	370

The terrain type is assumed as flat, open country, and since the meteorological weather station is close to the twin houses, the terrain is the same for both meteorological and local situations. The wind speed has been measured at z = 10 m. The height of the window in Child1 is estimated as 4.615 m based on the provided plans and elevations.

Assuming that the temperature and barometric pressure are constant over the building height, the volumetric flow resulting from stack effects, Q_s, is estimated as follows [13]:

$$Q_s = C_D A_{op} \sqrt{2g\Delta H_{NPL}(|T_{zone} - T_{odb}|/T_{zone})}$$

where C_D is the discharge coefficient, A_{op} is the opening area, g is the gravity force, T_{zone} is the zone temperature (room temperature), T_{odb} is the dry bulb temperature of the outside air, and ΔH_{NPL} is the height of neutral pressure level above reference plane without any other driving forces.

Estimating ΔH_{NPL} is a difficult task for naturally ventilated buildings. The ASHRAE Handbook of Fundamentals [13] suggests that *if one window or door represents a large fraction of the total opening area in the envelope, then the NPL is at the mid-height of that aperture, and ΔH_{NPL} equals one-half the height of the aperture*. A large fraction is considered as approximately 90 % of the total opening in the envelope. Since only the window in the Child1 room is open, this opening accounts for 100 % of the opening area, which validates the assumption of ΔH_{NPL} = H_{window}/2.

In the same case of a single opening, the interfacial mixing occurs across the counter-flow interface, and the discharge coefficient can be calculated according to the following equation (Kiel and Wilson 1986 [14] *and* ASHRAE Handbook of Fundamentals [13]):

$$C_D = 0.40 + 0.0045\,(T_{zone} - T_{odb})$$

As the windows only open in tilted position, the opening area is the product of the inward displacement (0.143 m) and the window width (1.23 m). As the window opens to the inside, the lateral sides of the window are sheltered by the wall (see Figure 1). Therefore, the lateral opening area is not added to the total opening area. Nevertheless, once the measurements are available, the model and its assumptions should be evaluated.

Figure 1: Window opens to the inside obstructing the lateral openings

Finally, the total ventilation rate is the root sum of the squared of the wind and stack airflow components as follow:

$$Q_T = \sqrt{Q_w^2 + Q_b^2}$$

2.8.5 Internal doors and trap door

During the experiment, most internal doors are left open, while some change position according to the phase in the experiment (corridor-sleeping room, trap door), or open and close following a particular schedule (kitchen-living). When these doors are open, an additional airflow between the different zones in the house could occur, which should be taken into account. This airflow could be caused by air pressure differences, which may originate from the mechanical ventilation and/or from temperature differences (natural ventilation).

As described in Section 2.6, airflow between the living room, corridor, bathroom and dining room as a result of the mechanical ventilation has been taken into account. The doors between these rooms are always open, and the airflow rate is assumed equal to the ventilation rate. The same is valid for the mechanical ventilation in the Child1 and Child2 rooms, in the attic.

A simplified modelling approach is used in this work to estimate the heat transfer caused by natural ventilation. The heat flux between two rooms is calculated as:

$$\dot{Q} = \dot{m}c_p\Delta T$$

where $\dot{m}$ is the airflow, c_p is the air heat capacity, and ΔT is the temperature difference between the rooms.

A power law relationship is used to estimate $\dot{m}$, as follows:

$$\dot{m} = A_{op}C_d\Delta P^n$$

where A_{op} is the opening area through which the air flows, C_d is the flow coefficient and n is the flow exponent. The opening area corresponds to the (trap) door area. A C_d of 0.5 is recommended for large openings. Turbulent flow has been assumed, for which n = 0.5. The implemented model assumes that the driving pressure, ΔP, results from the density difference between the two rooms.

The natural airflows considered in this work are the following:

1) Between kitchen and living, according to the schedule provided for the door position;
2) Between doorway and living (always open);
3) Between sleeping and corridor, according to the experiment phase;
4) Between living and staircase through the trap door, according to the experiment phase;
5) Between Child1 and staircase (always open);
6) Between Child2 and staircase (always open);

If airflow measurements become available from the tracer gas experiment, these could be used to evaluate the validity of the model. Moreover, when the airflow rate is known, the zone models in IDEAS allow the easy implementation of mass transfer between rooms.

The doors as components with a thermal mass and resistance (if closed), have been modelled as internal walls, as described in Section 2.4.5. For doors that are permanently open, both sides are connected to the same zone to which they open. The occasionally closed doors (kitchen-living, corridor-sleeping and trap door) were connected to both zones, thus assumed to be always closed, given that changing the connections between components and zones is not possible during the simulation.

2.8.6 Roller blinds

For most windows, the blinds are open permanently, while the blinds of the west facing windows of the ground floor are closed for a large part of the experiment, to minimize the influence of the different external shading on the two houses. While the specification document on Section 3.15.7 mentions that "west facing windows of the ground floor are always closed", Table 17 in the same document gives different information. It states that all blinds are open in the co-heating phase, the living room west window blinds are closed starting the User 1 phase, and the kitchen window blinds close starting the User 2 phase. This latter schedule has been programmed in our model, activating the shading effect of the blinds in the respective windows, namely blocking all solar gains, as described in Section 2.4.2.

2.8.7 Domestic Hot Water

Not included in the model.

2.9 WEATHER

This section described how the weather conditions that are not available in the measured data have been treated, including the solar model, sky temperature, and albedo. The measured data provides the global horizontal solar irradiation from which the direct and diffuse components are obtained for each orientation. The sky temperature is based on well-established models available in the literature. The albedo is calculated using the data from downward pyranometers, which measure the global solar irradiance reflected by the ground. The last part of this Section discuss the ground temperature.

2.9.1 Solar model

The direct beam radiation on the horizontal plane (E_{bh}) is derived from the global horizontal (E_{gh}) and the diffuse horizontal radiation (E_{dh}) in the climate file:

$$E_{bh} = E_{gh} - E_{dh}$$

The equations for the direct solar gains in Modelica are based on the beam radiation on the perpendicular surface (E_{bp}). The latter is calculated by:

$$E_{bp} = \frac{E_{bh}}{\cos(\omega)}$$

With ω the solar angle for the horizontal surface $(inc = 0°)$ given by:

$$\cos(\omega) = \cos(inc)\,(\cos(\delta)\cos(h)\cos(lat) + \sin(\delta)\sin(lat))$$
$$+ \sin(inc) * (\sin(azi) * \cos(\delta) * \sin(h) + \cos(azi) * (\cos(\delta)\cos(h) * \sin(lat) - \sin(\delta)\cos(lat))$$

With inc and azi the inclination and azimuth of the surface, δ the solar declination and h the solar hour, lat is the geographical latitude. The direct beam radiation on an inclined surface can then be calculated as:

$$E_{bs} = E_{bp}\cos(\omega_s)$$

With ω_s the solar angle on the inclined surface. Note that for numerical reasons the maximum of $\cos(\omega_s)$ and 0.001 are taken.

Finally, to calculate the diffuse irradiation on the tilted surfaces, the anisotropic sky model proposed by Perez et al. [15, 16] is used, for which the global horizontal and diffuse horizontal measured components are used as starting points.

2.9.2 Sky temperature

The sky is assumed to be an ideal black surface. The actual emittance of the clear and the clouded sky must be known. The effective sky temperature T_{sky} is then given as a function of the ambient temperature T_{amb}, the cloudiness factor of the sky, c_{cover}, and the emittance of the clear sky, ε_0:

$$T_{sky} = T_{amb}\varepsilon_0{}^{0.25} \quad [K]$$

The emittance of the clear sky, ε_0, can be derived by the dew point temperature (T_{dp}) corresponding the ambient conditions (temperature and air humidity) [1]:

$$\varepsilon_0 = 0.787 + 0.764 \ln\left(\frac{T_{dp}}{273.15}\right) C_a [-]$$

where C_a is a correction factor for estimating the influence of clouds, estimated by Clark and Allen (1987). C_a is a function of the cloudiness factor sky cover in tenths (N), as follows:

$$C_a = 1 + 0.0224\,N - 0.0035\,N^2 + 0.00028\,N^3 [-]$$

For clear sky conditions, N is equal to 0, and for overcast sky it is equal to 10. N is escalated from the cloudiness factor c_{cover}, which ranges between 0 and 1. Since the cloudiness factor c_{cover} is not given in the provided weather data file, it is estimated using the following correlation that depends on the ratio of diffuse to global radiation, respectively, E_{Diff} and $E_{Glob,H}$:

$$c_{cover} = \left(1.4286 \frac{E_{Diff}}{E_{Glob,H}} - 0.3\right)^{0.5} \quad [-]$$

2.9.3 Albedo

The albedo corresponds to the fraction of the solar irradiation that is reflected by the ground and, therefore, lies in the range between zero and one. In this work, the albedo is calculated as the ratio between the downwards solar irradiance and the global solar irradiance, both available in the measured data. The downwards irradiance has been measured in front of living room of each house (southwest side).

To calculate the albedo, the following two simplifications had to be made to handle unreliable and missing data:

1) In the beginning of the experiment, negative values occur in the downwards irradiance data of house O5. Moreover, before December 13, the downwards irradiation recorded at house O5 is close to zero. These data might indicate that the measurements at house O5 at the beginning of the experiment are not reliable. Therefore, a constant value equal to 0.23 is used for the period before December 13.

2) Downwards irradiance data are not available for house N2 at the beginning of the experiment. The data measured at house O5 is used to fill this gap (roughly the same period in which the albedo was assumed equal to 0.23).

The resulting albedo calculated for each house is presented in Figure 2 together with the snow height. A moving mean was used to smooth the data and reduce differences from one day to the other. The albedo is similar for both houses and follows the evolution of the snow height, with higher values for higher snow coverage. At the end of the experiment, this correlation is even more pronounced.
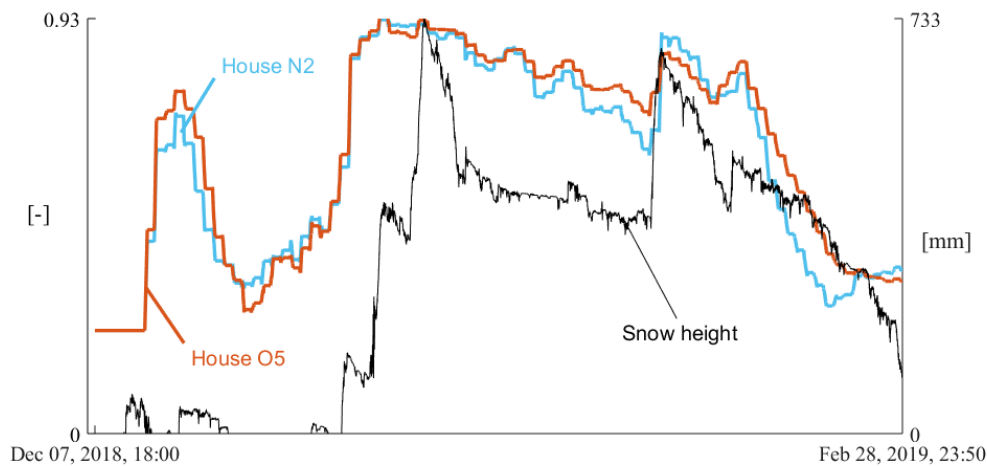
Figure 2: Calculated albedo for both houses.

2.9.4   Ground temperature

The ground temperatures were measured at different depths. This data, however, is not used since the basement is assumed to be at the given temperature and this is considered as boundary condition instead of the ground. For the longwave losses, the ground temperature is assumed equal to the air temperature (dry bulb).

3   RESULTS

This section gives an overview of the simulation results, in order to provide a first qualitative assessment of the correctness of the model. The presented results focus mainly on air temperatures and heat inputs, evaluated separately for each twin house. A thorough sensitivity analysis was not performed for this first report; however, the impact of including airflow coupling between zones through open doors was examined, and is shown in the results of house N2.

3.1   TWIN HOUSE N2

Twin house N2 is the base-case house, where all heating is electric. Without the additional complexity of the floor heating system, it is easier to assess the models in terms of zone air temperatures and heat inputs from the electric heaters. Since parts of the latter were already included for this house in the provided data (columns "*room_heat_elP*"), a comparison of the simulated and measured heat inputs is possible.

Figure 3 shows the zone air temperatures for most zones during the entire experiment (Co-heating, User 1 and User 2 phases), as well as the ambient air temperature and global horizontal radiation for the same period. Unheated zones are not shown, to avoid clattering the figure. Subsequent figures provide zoomed-in views on the different phases, or specific rooms.

We can easily distinguish the first Co-heating phase, where all zones are heated to 21°C. The PI control of the heaters manages to maintain the required temperature in all zones. Some peaks above the setpoint can be observed for some zones, mainly the living room, dining and kitchen, which result from higher ambient temperature and solar radiation peaks or high internal gains.
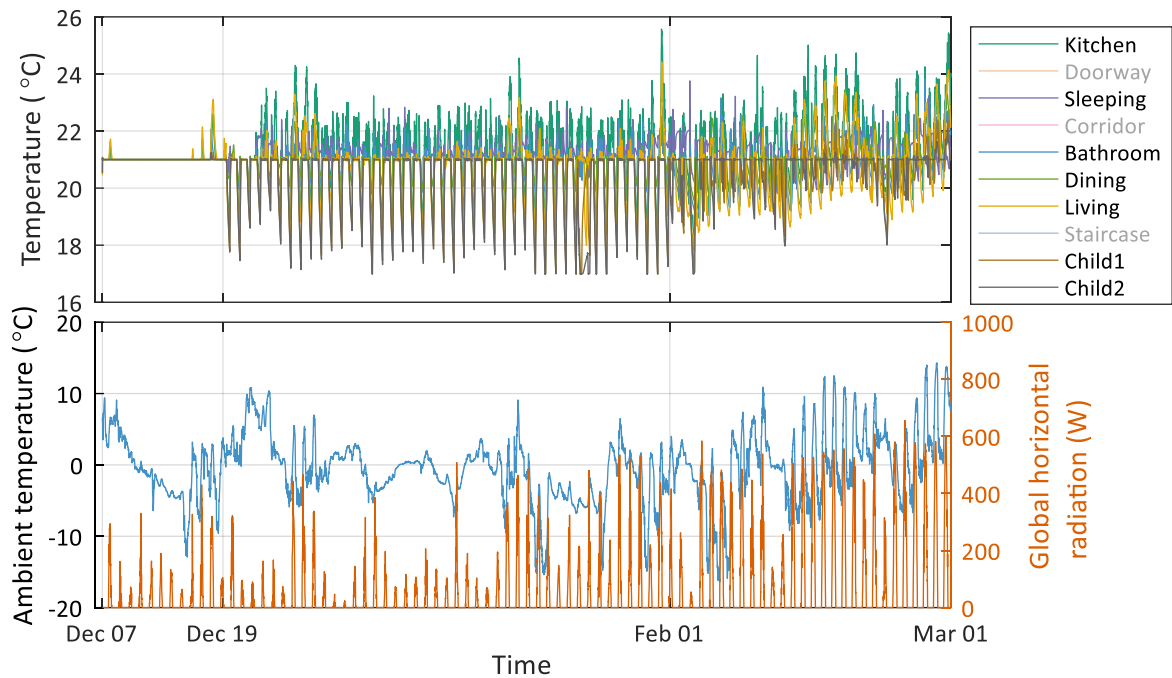
Figure 3: Air temperatures in heated zones of house N2 (top), and ambient temperature and global horizontal radiation (bottom).

During User 1 phase, all zones follow the same heating schedule, which is now variable, with a night set-back of 17°C. In this period, some rooms just manage to maintain the setpoint, such as the children's rooms, while the ground floor rooms often exceed this setpoint during the day, because of solar gains or internal heat sources. This is particularly pronounced for the kitchen, which has the higher internal gains, as shown in the zoomed-in view presented in Figure 4.
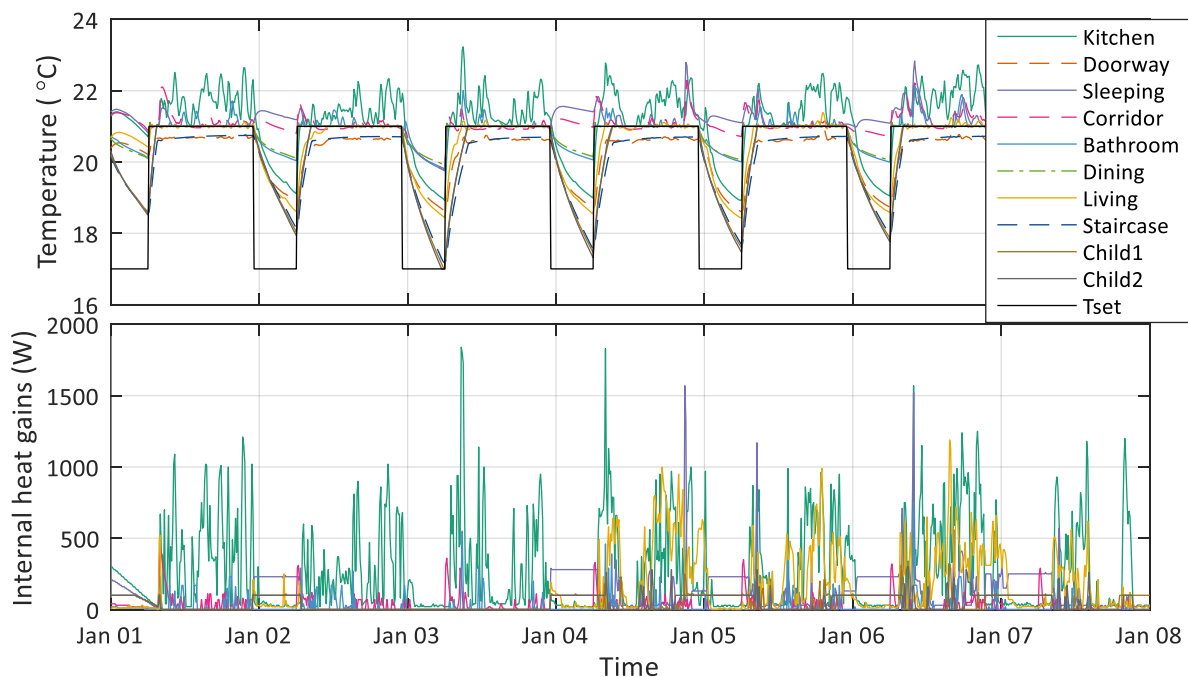
Figure 4: Air temperatures (top) and internal heat gains (bottom) for all zones during a week in User 1 phase in house N2. Unheated zones are plotted in dashed lines. The dining room is heated but has no internal heat gains.
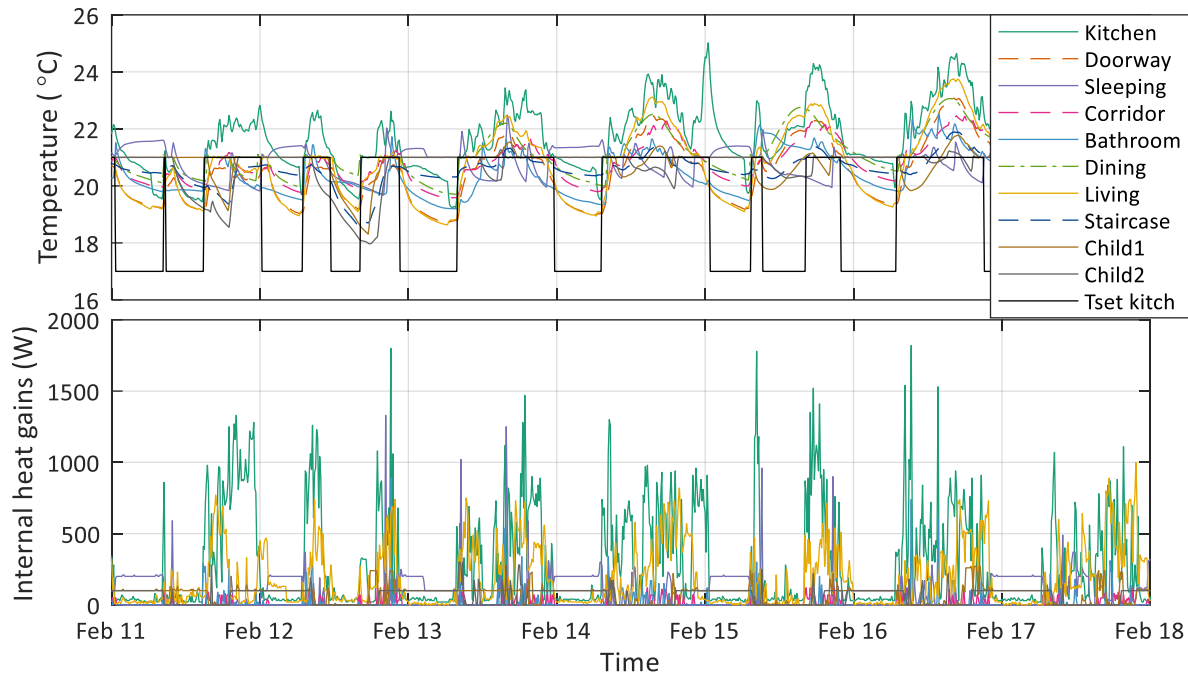
Figure 5: Air temperatures (top) and internal heat gains (bottom) for all zones during a week in User 2 phase in house N2. Unheated zones are plotted in dashed lines. The dining room is heated but has no internal heat gains. The set temperature for the kitchen is shown as an example, as the set points differ in each room.

In the last phase, User 2, each room follows its own heating schedule, which now coincides better with occupant presence and thus internal heat gains. Figure 5 shows a week in this phase, with an example of the heating schedule for the kitchen. More variation between rooms can be noticed. During this period, the temperature in all rooms is generally higher, which could be linked primarily to the warmer and sunnier weather, seen in Figure 3. The better coincidence of heating schedule and internal heat gains could be playing an additional role, as well as the fact that the trap door is open in this period, increasing the heat transfer from the living room to the upper floor. The effect of modelling open doors is further explained in the following.

As explained in Section 2.8.5, a model has been implemented to approximate the heat transfer between rooms when the internal door is open, and where no forced ventilation is present. This includes the following doors: corridor-sleeping room, trap door, kitchen-living, staircase-child 1 and staircase-child 2. To evaluate the effect that this model has, a comparison is made of simulation results with or without taking into account these interzonal heat transfers. Figure 6 shows the resulting temperature for some zones with (solid lines) and without this model (dashed lines). Note that the final results include the model. The bathroom and dining room are not included in the figure for clarity, since the difference is very small, and the forced ventilation airflows are included in both models anyway. We can see from this figure that the temperature of unheated rooms (corridor, doorway, staircase) increases significantly with the addition of the interzonal heat transfer, now following the trend of the setpoints in neighbouring rooms, though staying below this setpoint. The doorway's temperature increases a lot because of its connection to the living room. The corridor receives additional heat from the sleeping room, whose temperature decreases. The kitchen's temperature also decreases significantly, with only a limited increase in the living room's temperature. This is because the living room further loses heat to the corridor via forced ventilation. In this phase, the trap door is closed, so the staircase is mainly heated from its connection to the children's rooms.
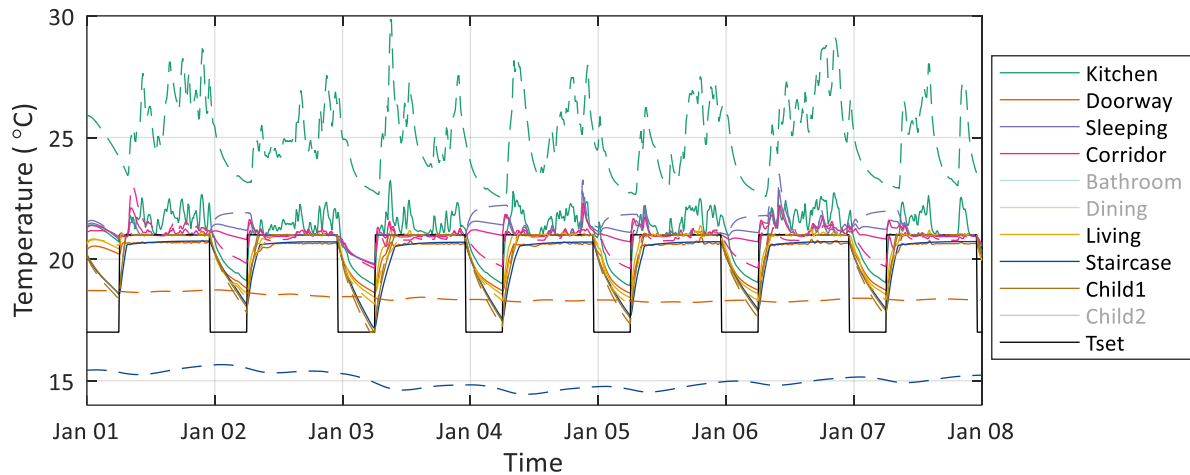
Figure 6: Comparison of the air temperature of some zones in house N2, using a model without interzonal heat transfer through open doors (dashed lines), and with interzonal heat flow (solid lines).

The following figures study the behaviour of specific rooms, additionally comparing the simulated heat inputs with the measured ones. Figure 7 shows the air temperature and heat inputs for three days in each of the User 1 and User 2 phases. We can observe that the gains from internal heat sources are very small compared to the required heating inputs. Furthermore, they are asynchronous with the heating schedule in User 1 phase, while they coincide in User 2 phase. The electric heating achieves to bring the temperature to the required level relatively fast. Comparing the measured and simulated heat inputs, there is a general agreement in both magnitude and shape. Some disagreement on the starting time of heating could be a result of different measured and simulated temperatures.
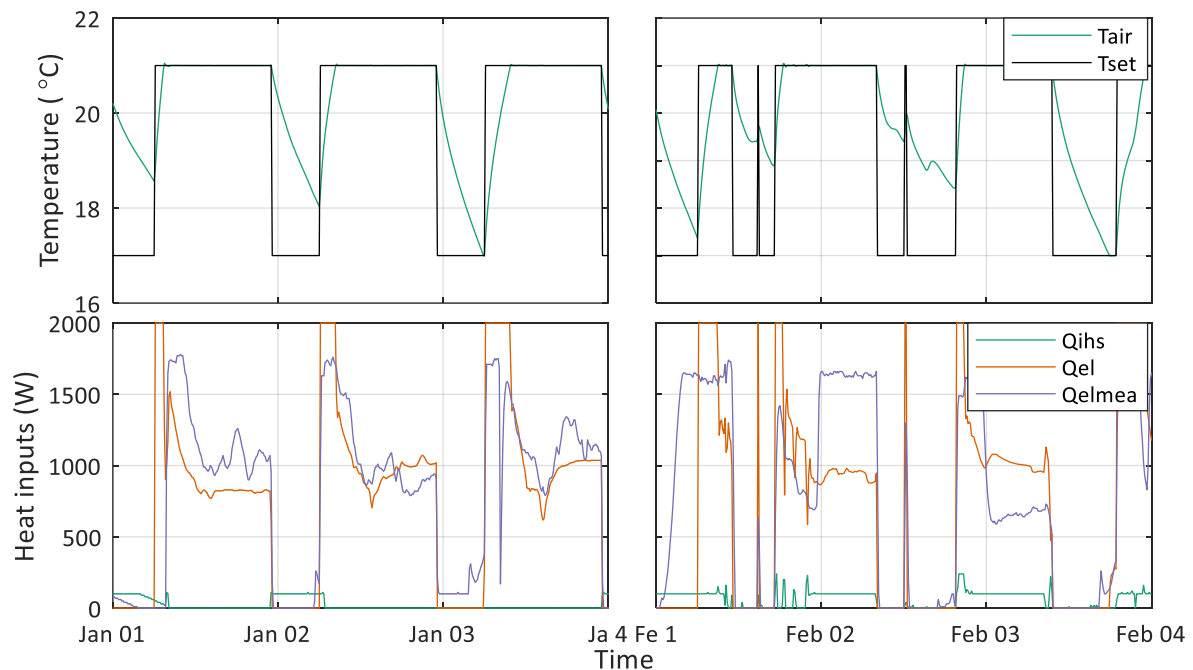

Figure 7: Detail on child 1 room in house N2. Air temperature and set point (top) and heat inputs from internal heat sources and the electric heating (bottom). The measured electric inputs from the provided data is also plotted for comparison. The plots show 3 days in User 1 phase (left) and 3 days in User 2 phase (right).
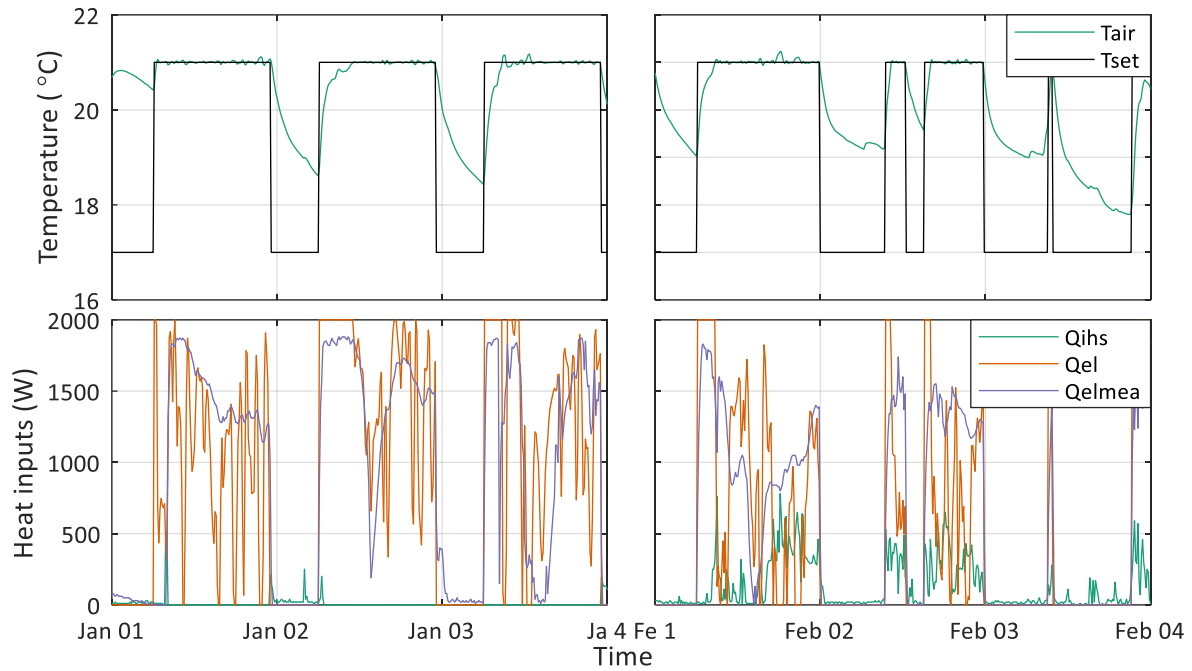
Figure 8: Detail on living room in house N2. Air temperature and set point (top) and heat inputs from internal heat sources and the electric heating (bottom). The measured electric inputs from the provided data is also plotted for comparison. The plots show 3 days in User 1 phase (left) and 3 days in User 2 phase (right).

Figure 8 and Figure 9 give the same results for the living room and kitchen respectively. We can notice that the living room requires much more heat to reach the setpoint than the kitchen, which barely needs any heating, given the high internal gains. For both rooms, the measured and simulated values are similar. Notice two occasions of sudden temperature drop in the kitchen during User 2 phase, caused by the scheduled opening of the internal door.
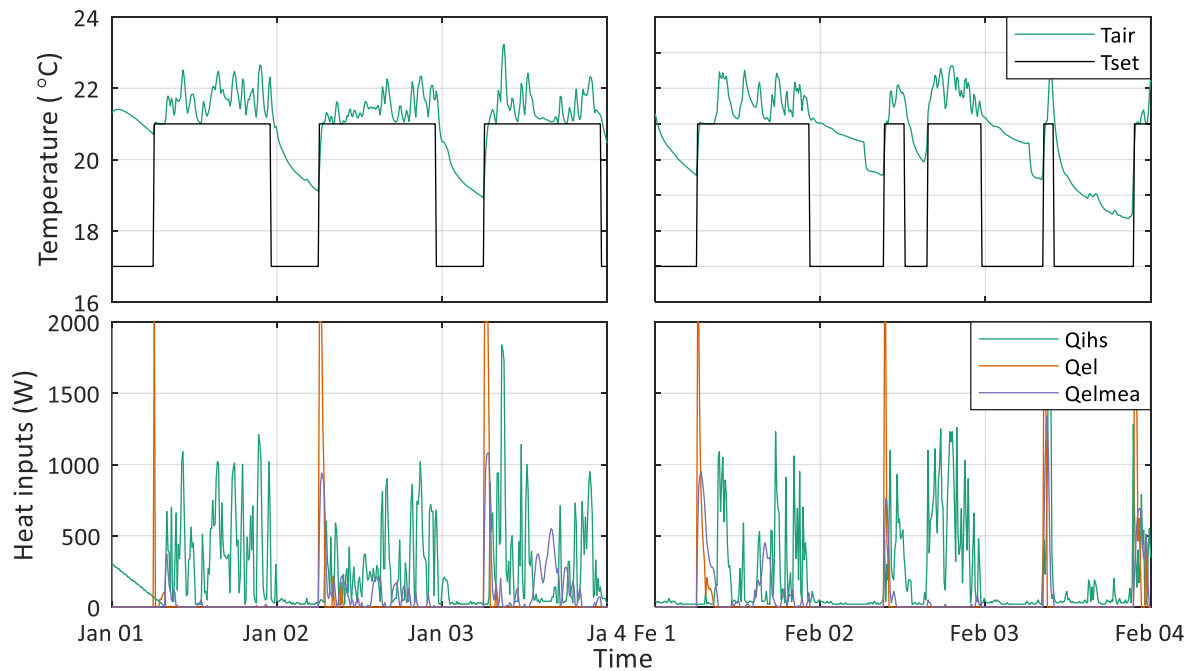

Figure 9: Detail on kitchen in house N2. Air temperature and set point (top) and heat inputs from internal heat sources and the electric heating (bottom). The measured electric inputs from the provided data is also plotted for comparison. The plots show 3 days in User 1 phase (left) and 3 days in User 2 phase (right).
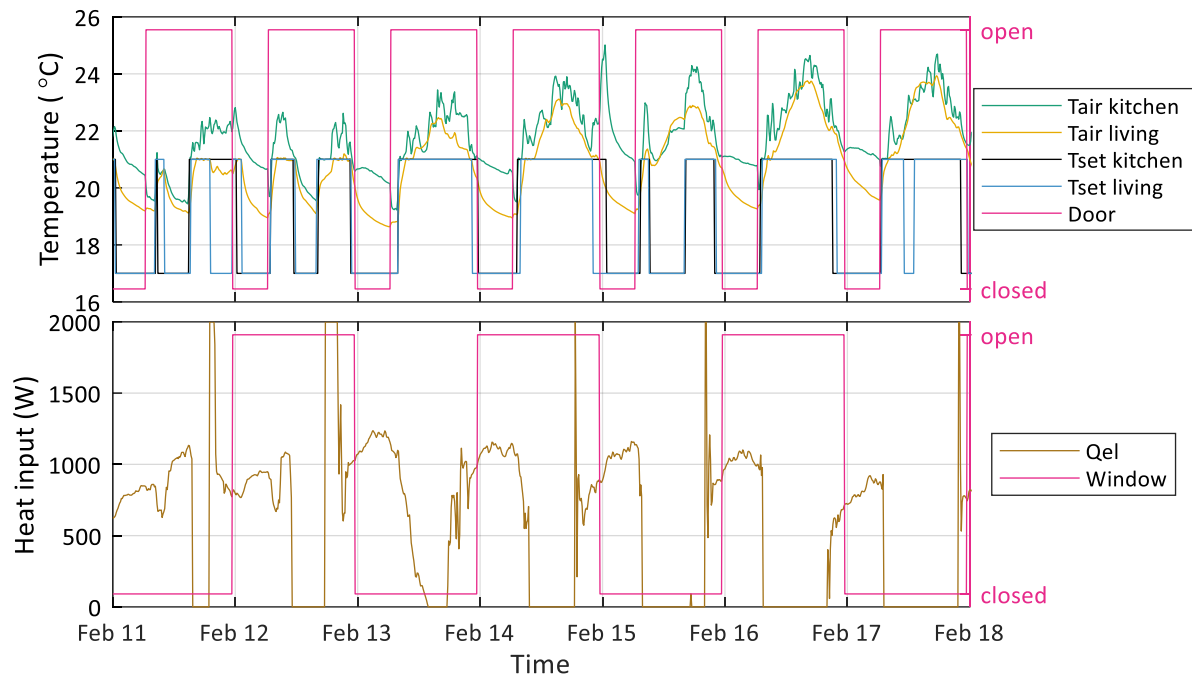
Figure 10: influence of internal door and external window opening on indoor air temperatures in the kitchen and living room (top), and the child 1 room (bottom) of house N2.

To better investigate the influence of opening the door between living room and kitchen, the upper plot of Figure 10 shows the temperature in both rooms during a week in User 2 phase. When the door is opened, the temperature of the kitchen immediately drops, while that of the living room increases momentarily. This is more visible around February 13, when the door opening does not coincide with the heating schedule. It would be beneficial to compare measurements with this simulation to assess whether this change in temperature would occur so fast and to this extent.

The bottom plot of Figure 10 examines the impact of opening the external window in child 1 room in the same period. Since the change of state happens during the heating phases, the change in temperature is not visible; therefore, the impact on the heating input is examined instead. When the window is opened, the heat input increases a bit in some of the days, while other times the change is not so pronounced. The difference could be related to the outdoor air temperature, which is about 5°C lower on February 14 and 16 compared to February 12.

3.2 TWIN HOUSE O5

The main difference between twin house O5 and N2 is the floor heating. As the heat pump was not modelled, the measured supply temperatures were used as input to the underfloor heating model. Since this approach allows no feedback between the actual temperature and the required heat input, it can be expected that any difference between the model and reality would cause the simulated temperature to deviate from the setpoint. The results presented in this section mainly focus on the behaviour of the floor heating system, as other aspects were treated for house N2.
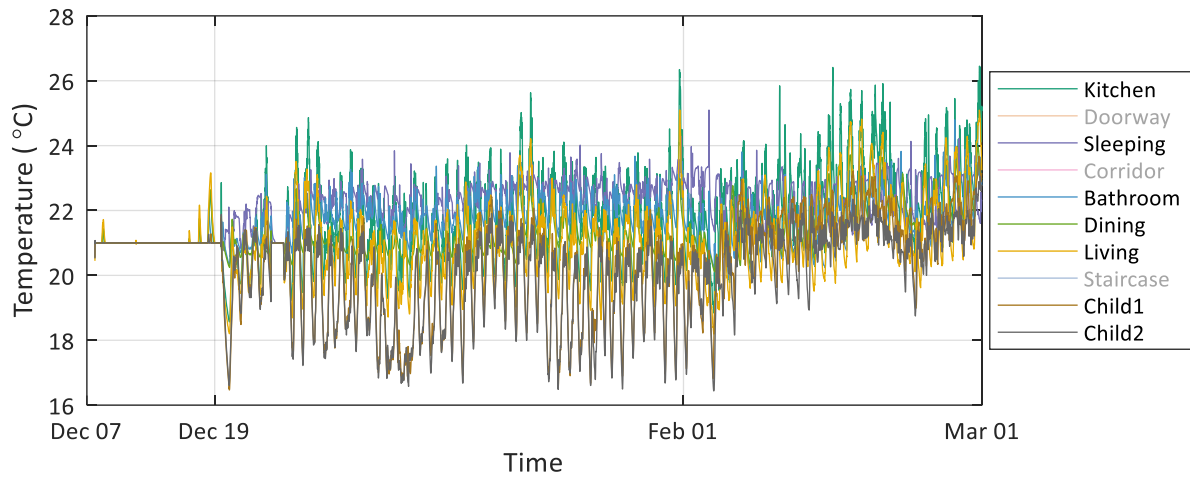
Figure 11: Air temperatures in heated zones of house O5.

Figure 11 shows a view of the temperature of heated zones throughout the experiment for house O5. Since the house uses electric heating for the Co-heating phase and few days around Christmas, the temperature in these periods follows the setpoint accurately, as for house N2. In phase User 1, the attic rooms tend to have temperatures below the setpoint, while the ground floor rooms are for most of the time above the setpoint, as also shown in Figure 12. This is in contrast to house N2, where the electric heating was able to maintain the setpoint in all rooms. In phase User 2, even the attic rooms begin to have temperatures regularly above the setpoint. An increase was also noticed in house N2, but to a lesser extent.
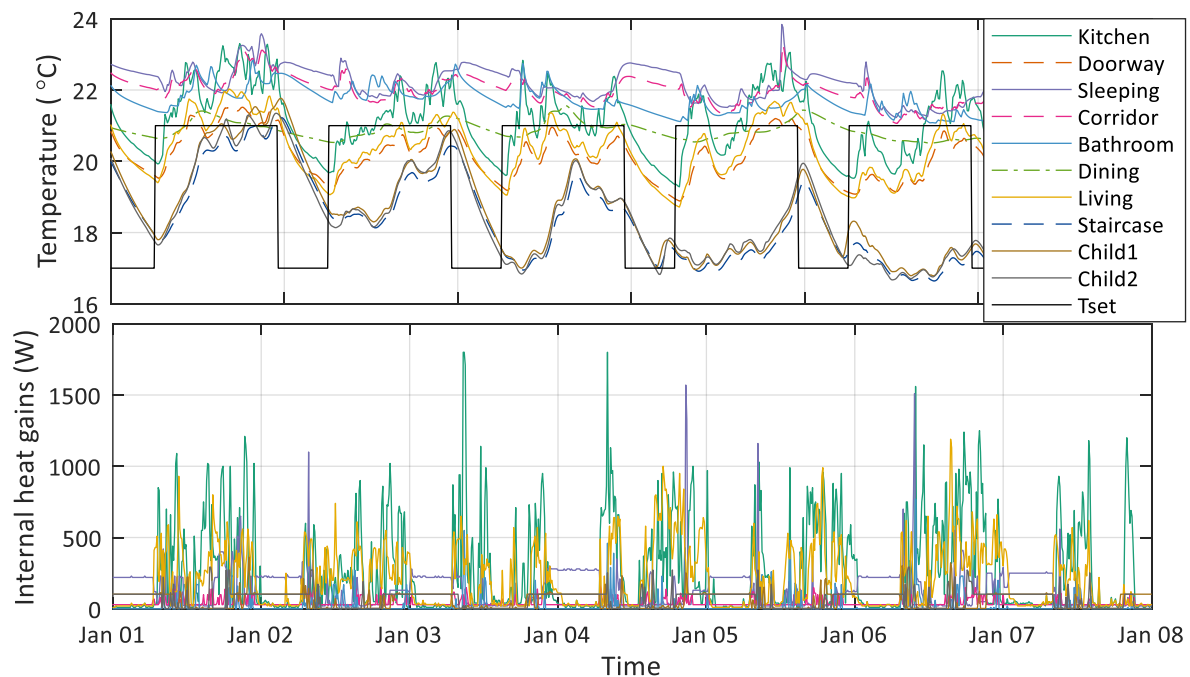

Figure 12: Air temperatures (top) and internal heat gains (bottom) for all zones during a week in User 1 phase in house O5. Unheated zones are plotted in dashed lines. The dining room is heated but has no internal heat gains.

Figure 13: Detail on living room of house O5 during a week in User 1 phase. Different temperatures of the zone and floor heating system (top), and heat inputs to the zone (bottom).

The exact reasons for the different behaviour between the attic and ground floor rooms are unclear. Internal heat gains are very dissimilar, but also the underfloor heating constructions differ. Figure 13 and Figure 14 show temperatures and heat inputs for the living room and child 1 room respectively. While supply temperatures are similar, the floor surface is cooler in the child 1 room, and the return temperature is higher. It is possible that the underfloor heating model does not accurately estimate the heat emission for one or both types of systems. Note that the return temperature is constant when the mass flow is zero, and the heat inputs are negative when the floor is warmer than the supply water.
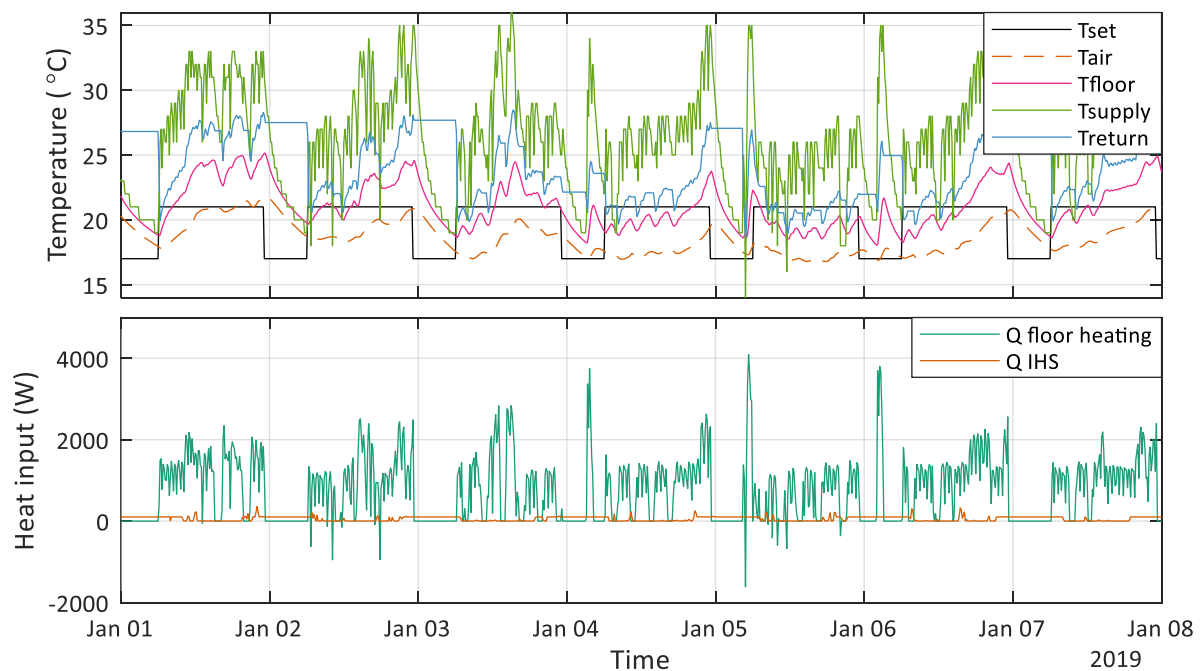

Figure 14: Detail on child 1 room of house O5 during a week in User 1 phase. Different temperatures of the zone and floor heating system (top), and heat inputs to the zone (bottom).

4 DISCUSSION AND SUGGESTIONS

In this Section, an overview of possible improvements of the model is given. To keep this report reasonably concise, sensitivity analyses are not presented here. Once the measurements are provided, several sensitivity analyses can be performed, as suggested below:

- **Internal heat sources**: During some periods of failure of the control system in the experiment, the internal heat gains in the houses were not following the normal schedule, as mentioned in Section 2.8.1. It is possible that some of the additional gains were not correctly implemented, as the results would suggest in Section 3.1. Therefore, some improvements could be made based on the measurements.
- **Influence of snow in the living room window**: The snow that causes shading on the glass door of the living room has not been modelled, since no data on the snow level at the glass door is available. Assuming that the frame of the glass door has the same thickness at the four sides, the frame is calculated to be 97 mm thick. The step in front of the door is assumed to be 200 mm based on the provided photographs. During nearly 60 % of the experiment, the measured snow level at the weather station was higher than 297 mm, with a maximum of 733 mm. The wind usually reduces the snow level at the south-oriented glass door, but the snow will probably cause some shading, although it expected to be of minor importance.
- **Thermal bridges**: Quantifying the impact of thermal bridges on the results is an interesting analysis since the calculation of thermal bridges has taken a significant amount of time and requested an equally significant amount of data.
- **Radiative/convective ratio of the heating system**: As discussed in Section 2.7.1, the fixed division between convective and radiant heat flows might affect the air temperature in the zones, since radiative and convective heat gains are treated differently.
- **Ventilation through the window**: The parameters used in Section 2.8.4 can influence significantly the amount of air entering the child room. The sensibility of the room temperature to the variation of the opening area, opening effectiveness or the discharge coefficient should be evaluated in future work.
- **Natural ventilation inside the houses**: The model described in Section 2.8.5 to represent the natural ventilation between rooms should be compared to the gas tracer results, as it has a significant impact on the temperatures inside the house. Alternatively, if tracer gas data is not available, the behaviour of measured temperatures can be compared to the schedule of internal doors to evaluate how well the model represents the actual air exchanges (similarly to the plots in Figure 10Figure 10: influence of internal door and external window opening on indoor air temperatures in the kitchen and living room (top), and the child 1 room (bottom) of house N2.).
- **Albedo**: Analysing the influence of the albedo on the results could be interesting, since this variable is typically assumed to be constant in building simulations.
- **Ground temperature**: The use of measured data in the calculation of the equivalent radiative environmental temperature requires the modification of the basic models in IDEAS library for outer components (outer walls, roof and windows). Future work should include this adaptation.
- **Heat pump modelling**: For this report, the modelling of the heat pump was not included. IDEAS Library has hydronic models that could be used in the future for this end.

REFERENCES

[1] openIDEAS, "Integrated District Energy Assessment Simulations," 2019. [Online]. Available: https://github.com/open-ideas.

[2] Dassault Systèmes, "Dymola Systems Engineering," [Online]. Available: https://www.3ds.com/products-services/catia/products/dymola/. [Accessed 01 08 2019].

[3] F. Jorissen, G. Reynders, R. Baetens, D. Picard, D. Saelens and L. Helsen, "Implementation and verification of the IDEAS building energy simulation library," *Journal of Building Performance Simulation,* pp. 669-688, 2018.

[4] R. Baetens, On externalities of heat pump based low-energy dwellings at the low-voltage distribution grid, KU Leuven, 2015.

[5] "DIN V 18599 (E) - Energy efficiency of buildings - Calculation of the net, final and primary energy demand for heating, cooling, ventilation, domestic hot water and lighting," 2016.

[6] J. A. Carroll, "An "MRT Method" of Computing Radiant Energy Exchange in Rooms," in *Systems Simulation and Economic Analysis*, San Diego, 1980.

[7] G. N. Walton, "Thermal Analysis Research Program Reference Manual," National Bureau of Standards, 1983.

[8] Ubakus, "U-wert rechner," [Online]. Available: https://www.ubakus.de/u-wert-rechner/. [Accessed 01 08 2019].

[9] S. Salavation, M. D'Orazio, C. Di Perna and E. Di Giuseppe, "Assessment of Cardboard as an Environment-Friendly Wall Thermal Insulation for Low-Energy Prefabricated Buildings," in *Sustainable Building for a Cleaner Environment*, 2019, pp. 463-470.

[10] Cooke Brothers, "Door weights," [Online]. Available: https://www.cookebrothers.co.uk/technical/product-performance/door-weights. [Accessed 01 08 2019].

[11] M. Koschenz and B. Lehmann, Thermoaktive Bauteilsysteme tabs, EMPA, 2000, p. 102.

[12] M. S. Owen, ASHRAE Handbook: Fundamentals, ASHRAE, 2009.

[13] ASHRAE, ASHRAE Handbook: Fundamentals, ASHRAE, 1989.

[14] D. E. Kiel and D. J. Wilson, "Gravity driven flows through open doors," in *7th AIVC Conference*, 1986.

[15] R. Perez, R. Seals, P. Ineichen, R. Stewart and D. Menicucci, "A New Simplified Version of the Perez Diffuse Irradiance Model for Tilted Surface," *Solar Energy,* 1987.

[16] R. Perez, P. Ineichen, R. Seals, J. Michalsky and R. Stewart, "Modeling Dyalight Availability and Irradiance Componets From Direct and Global Irradiance," *Solar Energy,* vol. 44, no. 5, pp. 271-289, 1990.

[17] J. Thomas, "Thermal Properties of Paper," Sciencing, [Online]. Available: https://sciencing.com/thermal-properties-paper-6893512.html. [Accessed 01 07 2019].

[18] E. Di Giuseppe and M. D'Orazio, "Assessment of the effectiveness of cool and green roofs for the mitigation of the Heat Island effect and for the improvement of thermal comfort in Nearly Zero Energy Building," *Architectural Science Review,* vol. 5, no. 2, pp. 134-143, 2015.